A low-temperature study of manganese-induced ferromagnetism and valence band convergence in tin telluride

Hang Chi,[1,2,a)] Gangjian Tan,[3] Mercouri G. Kanatzidis,[3] Qiang Li,[2] and Ctirad Uher[1]

[1]*Department of Physics, University of Michigan, Ann Arbor, Michigan 48109, USA*
[2]*Condensed Matter Physics and Materials Science Department, Brookhaven National Laboratory, Upton, New York 11973, USA*
[3]*Department of Chemistry, Northwestern University, Evanston, Illinois 60208, USA*

SnTe is renowned for its promise in advancing energy-related technologies based on thermoelectricity and for its topological crystalline insulator character. Here, we demonstrate that each Mn atom introduces $\sim 4\,\mu_B$ (Bohr magneton) of magnetic moment to $Sn_{1-x}Mn_xTe$. The Curie temperature T_C reaches $\sim 14\,K$ for $x = 0.12$, as observed in the field dependent hysteresis of magnetization and the anomalous Hall effect. In accordance with a modified two-band electronic Kane model, the light L-valence-band and the heavy Σ-valence-band gradually converge in energy with increasing Mn concentration, leading to a decreasing ordinary Hall coefficient R_H and a favorably enhanced Seebeck coefficient S at the same time. With the thermal conductivity κ lowered chiefly via point defects associated with the incorporation of Mn, the strategy of Mn doping also bodes well for efficient thermoelectric applications at elevated temperatures. *Published by AIP Publishing.*
[http://dx.doi.org/10.1063/1.4948523]

SnTe crystallizes in the $Fm\bar{3}m$ $(O_h^5$, No. 225) structure with lattice parameter $a = 6.318\,\text{Å}$,[1,2] well known for thermoelectric (TE) applications.[3–16] The band gap, separating the conduction band (CB) and the light valence band (LVB), is located at the L point of the Brillouin zone. Another heavy valence band (HVB), also contributing to transport, is present at the Σ point, with an energy offset $\Delta E \sim 0.3$–$0.4\,\text{eV}$.[17,18] The properties of SnTe depend critically on Sn vacancies (V''_{Sn}, double-hole acceptors), which lead to $\sim 10^{20}\,\text{cm}^{-3}$ holes in "pristine" SnTe.[19] Recently, SnTe has been identified as a topological crystalline insulator (TCI).[20,21] Its surface states (SSs) are topologically protected by the crystalline symmetry,[22] in contrast to topological insulators (TIs)[23,24] where magnetic dopants break the time-reversal symmetry and open up a gap in the SSs.[25–27] Introducing magnetism in SnTe is thus of fundamental interest as it may realize phenomena such as the quantum anomalous Hall effect.[28–30] Doping SnTe with manganese seems promising, as is known in dilute magnetic semiconductors (DMSs) including II-VI,[31,32] III-V,[33,34] IV(-VI),[35,36] and V_2VI_3 compounds.[37] Although Mn gives rise to ferromagnetism in SnTe, earlier studies have only examined samples with either too low Mn content ($\ll 10\,\text{at. }\%$)[38] or too high hole concentrations.[39] More comprehensive low-temperature magnetic and transport characterizations on a wider range of Mn concentrations are desirable.

Here, we report our recent study on $Sn_{1-x}Mn_xTe$ ($x = 0$–0.12), where the Curie temperature T_C increases as a function of x. Consistent with a two-band Kane model and a Debye-Callaway thermal conductivity formula, the low-temperature transport properties evolve systematically upon Mn doping, which suggests the convergence of the L and Σ bands, favoring efficient thermoelectricity.

Polycrystalline $Sn_{1-x}Mn_xTe$ ($x = 0$–0.12) were synthesized and structurally characterized as detailed in Ref. 8. The X-ray diffraction (XRD) measurements have detected no secondary phases. The samples studied here can be treated as single phase at the XRD level, although transmission electron microscopy (TEM) studies have revealed the presence of a small amount of Mn-rich nanoinclusions for $x = 0.12$.[8] This suggests that the solubility limit of Mn in SnTe is $x \sim 0.12$. Rectangular bar-shaped samples ($\sim 1.5 \times 2.5 \times 5.5\,\text{mm}^3$) were cut out at room temperature using a diamond saw. Magnetic and transport measurements were performed over the temperature range of 1.8–300 K. Magnetic studies were conducted using a superconducting quantum interference device (SQUID) magnetometer equipped with a 5.5 T magnet in a Quantum Design Magnetic Property Measurement System (MPMS). The electrical resistivity ρ, Seebeck coefficient S, and thermal conductivity κ were determined using a longitudinal steady-state technique.[40] Hall effect and magnetoresistance (MR) measurements were performed using a Linear Research ac bridge with 16 Hz excitation. The uncertainties of ρ, S, and κ are $\pm 3\%$, $\pm 2\%$, and $\pm 5\%$, respectively.

The temperature dependent susceptibilities χ_m ($= M/H$ per mole) in an applied magnetic field $H = 40\,\text{Oe}$ (magnetization M depends linearly on H up to $\sim 50\,\text{Oe}$) are plotted in Fig. 1. With $x > 0.03$, the system becomes ferromagnetic, manifesting a significant increase of χ_m below $\sim 20\,K$. As shown in the upper inset of Fig. 1, above T_C, χ_m for $x \geq 0.03$ follows the Curie-Weiss law

$$\chi_m = \frac{C}{T - \theta_p} + \chi_0, \tag{1}$$

where C is the Curie constant, T is the absolute temperature, θ_p is the paramagnetic Curie temperature, and χ_0 is a lattice term. The fitting parameters are summarized in Table I, together with the effective moment per Mn atom, p_{eff}, deduced

a)Author to whom correspondence should be addressed. Electronic mail: chihang@bnl.gov.
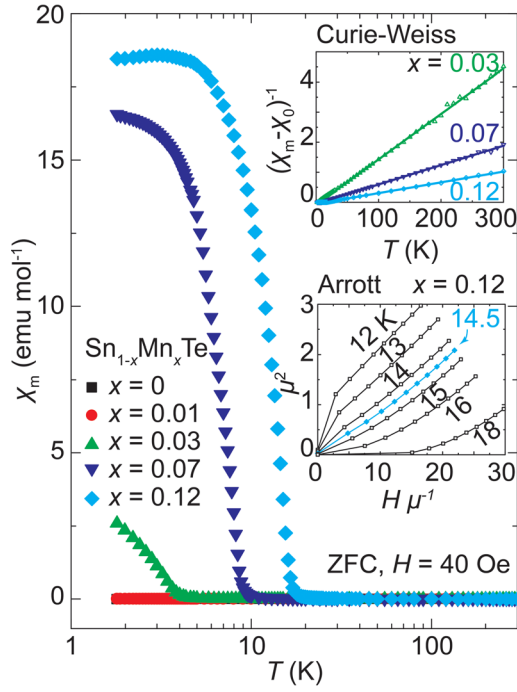
FIG. 1. Zero-field-cooled (ZFC) χ_m measured with $H = 40$ Oe for $Sn_{1-x}Mn_xTe$. The susceptibilities are well described (upper inset) by the Curie-Weiss law. The θ_p agrees with T_C determined from the Arrott plot, as exemplified for $x = 0.12$ (lower inset).

from $C = N_A p_{eff}^2 \mu_B^2 / 3k_B x$, where N_A is the Avogadro's number, μ_B is the Bohr magneton, and k_B is the Boltzmann constant. As exemplified in the lower inset of Fig. 1 for $x = 0.12$, T_C can be determined via the Arrott plot (μ^2 vs. $H\mu^{-1}$),[41] in reasonable agreement with θ_p. Future studies are needed to clarify the contribution to the magnetic response from the nanoinclusions at the grain boundaries of $x = 0.12$. Furthermore, doping beyond the bulk solubility limit $x \sim 0.12$, using non-equilibrium technique such as molecular beam epitaxy (MBE), may achieve even higher T_C, considering T_C of V-doped Sb_2Te_3 was successfully improved from 22 K (bulk $Sb_{1.97}V_{0.03}Te_3$) to 177 K ($Sb_{1.65}V_{0.35}Te_3$ thin film).[42]

As shown in Fig. 2(a), M of SnTe displays linear field dependence at 1.8 K. With increasing x, hysteresis gradually develops and the high-field saturated M (up to 10 kOe) has quickly reached values exceeding 2000 emu mol^{-1} for $x = 0.12$. Measurements at low fields reveal small coercivity fields $H_C \sim 10$ Oe, indicating the softness of these ferromagnetic semiconductors.
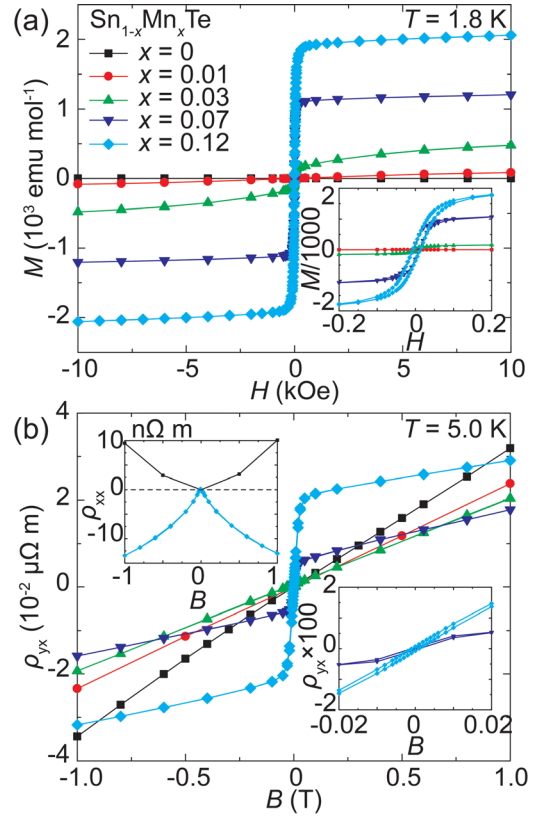

FIG. 2. (a) The field dependent M for $Sn_{1-x}Mn_xTe$ at $T = 1.8$ K showing a hysteresis loop with $H_C \sim 10$ Oe (inset). (b) The ρ_{yx} ($T = 5.0$ K) of $Sn_{1-x}Mn_xTe$ develops hysteresis (anomalous Hall effect) for $x = 0.07$ and 0.12 (lower-right inset). The linearity and the decreasing slope at higher fields indicate a decreasing R_H upon Mn doping. The upper-left inset compares the MR in samples with ($x = 0.12$) and without Mn ($x = 0$).

M contributes to the Hall resistivity ρ_{yx} via

$$\rho_{yx} = R_H B + R_s M, \qquad (2)$$

where R_H is the ordinary Hall coefficient, B ($=\mu_0 H$) is the magnetic induction, and R_s is the anomalous Hall coefficient. The second term disappears well above T_C, restoring linear field dependence for ρ_{yx}. The presence of R_s revealed in the hysteretic behavior of ρ_{yx} vs. B is one of the most reliable proofs of ferromagnetism. As shown in Fig. 2(b), a distinctly hysteretic character of ρ_{yx} is apparent with $x > 0.03$ at 5.0 K. The very low coercivity [lower inset in Fig. 2(b)] corroborates the M vs. H hysteresis loops in the inset of Fig. 2(a). Considering that M is already well saturated above

TABLE I. Fitting results of $Sn_{1-x}Mn_xTe$. The magnetic parameters C (emu K mol^{-1}), θ_p (K), χ_0 (10^{-5} emu mol^{-1}), p_{eff} (per Mn), and T_C (K) are from the Curie-Weiss law. The electronic properties ρ ($\mu\Omega$ m), S (μV K^{-1}), R_H (10^{-2} cm^3 C^{-1}), μ_H (cm^2 V^{-1} s^{-1}), E_g (eV),[1,52] ΔE (eV), and L (10^{-8} W Ω K^{-2}) are from experiments or the two-band Kane model at 300 K. The thermal coefficients ℓ (μm), A (10^{-41} s^3), and U (10^{-17} s K^{-1}) are based on the Debye-Callaway formula.

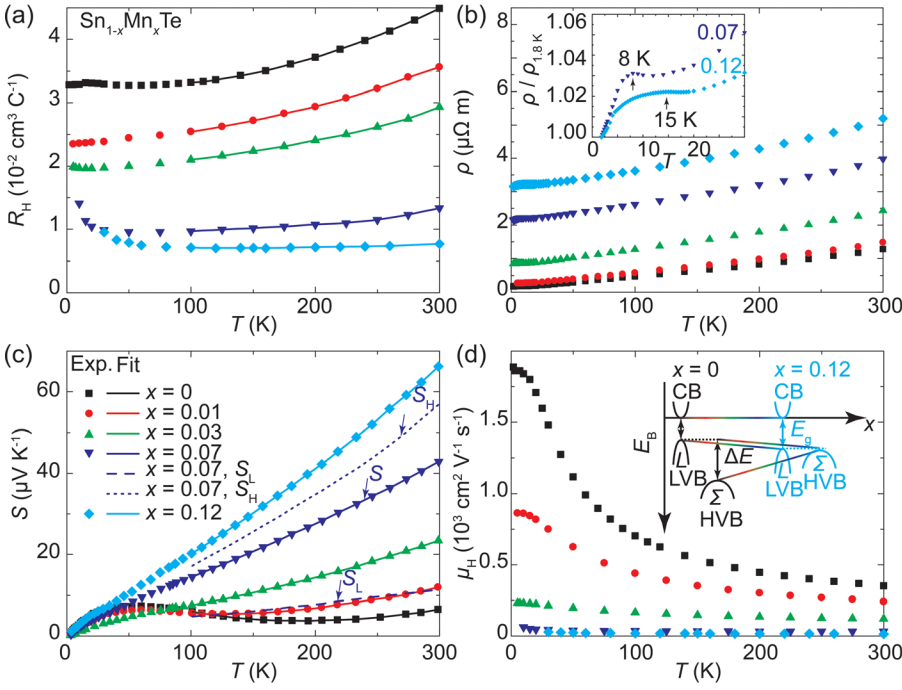|	Magnetic					Electronic							Thermal		
x	C	θ_p	χ_0	p_{eff}	T_C	ρ	S	R_H	μ_H	E_g	ΔE	L	ℓ	A	U
0	…	…	…	…	…	1.28	6.48	4.49	351	0.18	0.43	2.49	2.12	0.98	0.86
0.01	…	…	…	…	…	1.48	11.9	3.56	241	0.19	0.40	2.59	2.01	1.43	0.87
0.03	0.066	5.48	−1.62	4.20	1.8	2.43	23.4	2.93	121	0.21	0.36	2.56	0.66	2.41	0.83
0.07	0.155	7.94	−1.13	4.21	7.5	3.98	42.9	1.33	33.4	0.26	0.14	2.27	0.95	3.83	1.01
0.12	0.279	15.1	2.74	4.31	14.5	5.19	66.2	0.77	14.8	0.31	−0.10	2.12	1.71	4.75	1.73

FIG. 3. The temperature dependent (a) R_H, (b) ρ, (c) S, and (d) μ_H of $Sn_{1-x}Mn_x$ Te. The inset of (b) shows that ρ of ferromagnetic samples ($x = 0.07$ and 0.12) develops a peak at $\sim T_C$. The inset of (d) summarizes the band structure (binding energy E_B at high symmetry points L and Σ). The LVB (at L) and HVB (at Σ) converge in energy upon Mn doping, leading to a much enhanced S. The numerical fitting (lines) in (a) and (c) simultaneously account for both R_H and S within a two-band Kane model. For $x = 0.07$, the two-band S is compared with contributions from its single-band components S_L (from LVB) and S_H (from HVB).

$H \sim 1$ kOe and possesses little field dependence at high fields, the decreasing slope of ρ_{yx} in its high-field linear region is mainly due to the decreasing magnitude of R_H as x increases. The R_H can be extracted from the linear field dependence of ρ_{yx} above T_C and is displayed in Fig. 3(a). Furthermore, the alignment of spins in Mn-doped samples (e.g., $x = 0.12$) in the presence of B leads to a negative MR, in contrast to the positive semi-classical parabolic MR of SnTe [upper inset in Fig. 2(b)].

The temperature dependent electronic properties of $Sn_{1-x}Mn_x$Te are illustrated in Fig. 3, with 300 K values collected in Table I. Due to the high apparent hole concentration p_H ($\equiv 1/eR_H$, e being the elementary charge) $\sim 1.9 \times 10^{20}$ cm^{-3} (10 K), ρ of SnTe [Fig. 3(b)] is metallic. While S of SnTe exhibits a nearly linear temperature dependence close to ambient temperatures (dominated by diffusion processes), at low temperatures it develops a broad peak at ~ 50 K which originates from strong electron-phonon coupling referred to as the phonon-drag effect.[43] Acoustic phonons responsible for this effect also produce a dielectric maximum observed on κ in Fig. 4(a). The phonon drag is substantially washed out with increasing Mn, which strongly scatters acoustic phonons.

While the carrier density measured by R_H, assuming a single parabolic band, clearly increases with increasing x, the Hall mobility μ_H ($\equiv R_H/\rho$) rapidly diminishes [Fig. 3(d)] and is responsible for the rising ρ. Meanwhile, S gradually improves with increasing x [Fig. 3(c)]. This might seem to be a consequence of lowered Fermi level E_F in a single band with the density of states $D(\varepsilon)$, where ρ and S are proportional to $D(\varepsilon)^{-1}$ and $\partial \ln D(\varepsilon)/\partial \varepsilon$, respectively.[44,45] However, such a naïve scenario should be accompanied by a decrease in p_H, contradicting its increase as the R_H data clearly suggest.

Considering both LVB and HVB [inset of Fig. 3(d)], the overall two-band[46–48] electronic properties (R_H, S, and the Lorenz number L) are combinations of single-band components

$$R_H = \frac{R_{H,L}p_{N,L}^2 b^2 + R_{H,H}p_{N,H}^2}{(p_{N,L}b + p_{N,H})^2}, \qquad (3)$$

$$S = \frac{S_L p_{N,L}b + S_H p_{N,H}}{p_{N,L}b + p_{N,H}}, \qquad (4)$$

$$\text{and } L = \frac{L_L p_{N,L}b + L_H p_{N,H}}{p_{N,L}b + p_{N,H}} + \frac{p_{N,H}p_{N,L}b(S_H - S_L)^2}{(p_{N,L}b + p_{N,H})^2}, \qquad (5)$$
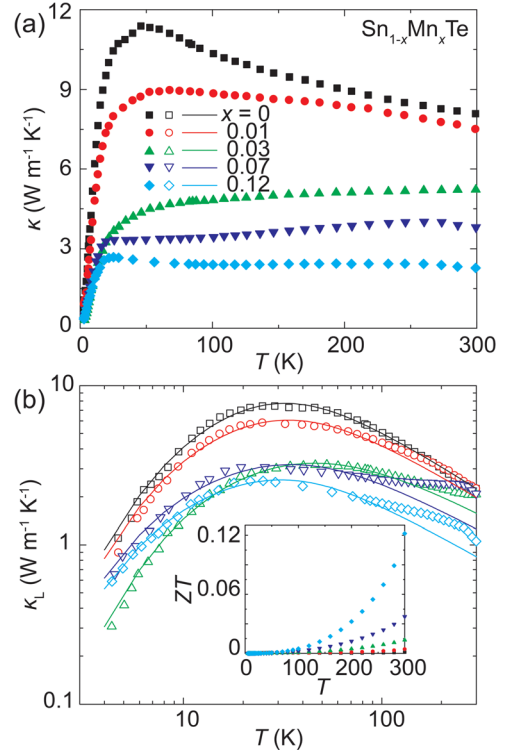

FIG. 4. (a) The temperature dependent κ of $Sn_{1-x}Mn_x$Te. (b) The κ_L is well understood within the Debye-Callaway phonon conductivity model, revealing the enhanced point defect scattering upon Mn doping. The inset in (b) illustrates the dramatically improved ZT at room temperature for the most heavily doped sample, suggesting that efficient TE applications based on these compounds are possible at high temperatures.

respectively. The mobility ratio b ($\equiv \mu_L/\mu_H$) is taken to be 8 for SnTe according to Ref. 18. In a single Kane band with nonparabolicity parameter β ($\equiv k_B T/E_g$), the number concentration of holes p_N is given by

$$p_N = \frac{(2m_d^* k_B T)^{3/2}}{3\pi^2 \hbar^3} \, {}^0F_0^{3/2}, \qquad (6)$$

where m_d^* is the density-of-states effective mass and $\hbar$ is the reduced Planck constant. Assuming acoustic phonon dominates,[49–51] the generalized Fermi integrals are

$$^n F_k^m (\eta) = \int_0^\infty \left(-\frac{\partial f_0}{\partial \xi} \right) \xi^n (\xi + \beta \xi^2)^m [(1 + 2\beta\xi)^2 + 2]^{k/2} d\xi, \qquad (7)$$

where $f_0 = (e^{\xi - \eta} + 1)^{-1}$ is the Fermi-Dirac distribution, $\xi = \varepsilon/k_B T$, and $\eta = \mu_c/k_B T$, with the energy ε and chemical potential μ_c measured from the band edge and $\Delta E = k_B T (\eta_L - \eta_H)$. The single Kane-band electronic properties are

$$R_H = \frac{1}{e p_N} \frac{{}^0F_{-4}^{1/2} \cdot {}^0F_0^{3/2}}{({}^0F_{-2}^1)^2}, \qquad (8)$$

$$S = \frac{k_B}{e} \left[\frac{{}^1F_{-2}^1}{{}^0F_{-2}^1} - \eta \right], \qquad (9)$$

$$\text{and } L = \left(\frac{k_B}{e} \right)^2 \left[\frac{{}^2F_{-2}^1}{{}^0F_{-2}^1} - \left(\frac{{}^1F_{-2}^1}{{}^0F_{-2}^1} \right)^2 \right], \qquad (10)$$

respectively.

Assuming a Kane-like LVB and a parabolic HVB ($\beta_H = 0$),[3,4,47,48] the two-band Kane model [solid lines in Figs. 3(a), 3(c)] is used to characterize the temperature and composition dependence of R_H and S, with a temperature-dependent E_g[1,52] and constant effective masses (in the unit of rest electron mass m_e) $m_{d,L}^* = 0.1$ and $m_{d,H}^* = 3$, respectively. The fitting parameters are displayed in Table I. A universal shrinking trend (insensitive of E_g and m_d^*) of ΔE vs. x (from $\sim$0.40 eV for SnTe to a somewhat negative value for $x = 0.12$) has been observed, indicating that Mn gradually changes the band structure and brings into energy convergence the two valence bands–consistent with recent theories.[8] An ability to achieve band convergence via chemical doping is beneficial for further improving the TE performance of SnTe,[5,53,54] as the temperature-induced convergence in PbTe [$\Delta E \sim 0.17$ eV (Ref. 55)] is much less feasible in SnTe due to its considerably larger ΔE. As illustrated in Fig. 3(c), contributions to S from the LVB (S_L) and HVB (S_H) are compared with the total S for $x = 0.07$. The data suggest that holes are transferred from the LVB to HVB due to the band convergence. Indeed, the less mobile holes in the HVB become more dominant in the electrical transport, leading to an enhanced S and reduced μ_H.

The κ of $Sn_{1-x}Mn_xTe$ decreases with increasing x essentially over the whole measured temperature range, as shown in Fig. 4(a). The peak in κ of SnTe is drastically suppressed due to strong phonon scattering by Mn. The lattice thermal conductivity κ_L, estimated by subtracting the electronic thermal conductivity κ_e (=LT/ρ, according to the Wiedemann-Franz

law) from κ, has been examined using the Debye-Callaway model[40]

$$\kappa_L = \frac{k_B}{2\pi^2 v} \left(\frac{k_B}{\hbar} \right)^3 T^3 \int_0^{\theta_D/T} \frac{x^4 e^x}{(e^x - 1)^2} \times \frac{1}{v/\ell + A\omega^4 + U\omega^2 T \exp(-\theta_D/3T)} dx, \qquad (11)$$

where $x = \hbar\omega/k_B T$, ω is the phonon frequency, v ($\sim$2000 m s^{-1}) is the averaged sound velocity,[56] θ_D ($\sim$177 K) is the Debye temperature,[57] ℓ is the mean grain size, A represents the Rayleigh point defect scattering, and U denotes the Umklapp processes.[58] As shown in Fig. 4(b), the phonon conductivity model describes reasonably well the temperature dependence of κ_L. However, future effort is needed to improve the model presented here, in order to consider effects from nanoinclusions.[59] The fitting parameters are summarized in Table I, revealing a clear trend of enhanced point defect scattering (A) with increasing Mn. The fitted ℓ is approximately on par with the values (5–10 μm) typically observed in our SnTe-based polycrystalline samples.[8]

The synergistically tuned electrical and thermal transport properties give rise to an enhanced TE figure of merit ZT [$\equiv S^2 T/\rho\kappa$, inset of Fig. 4(b)]. At room temperature, the ZT for $x = 0.12$ ($\sim$0.1), two orders of magnitude higher than that of SnTe, holds promise for TE performance. Indeed, high ZT values $\sim$1.3 (900 K) for $Sn_{1-x}Mn_xTe$ have been recently reported.[8–11]

In summary, magnetic and transport studies have been performed on $Sn_{1-x}Mn_xTe$, with x approaching the bulk solubility limit $\sim$0.12. T_C of $\sim$14 K has been achieved for $x = 0.12$ in the ferromagnetically doped SnTe, as confirmed via the hysteresis in both magnetization and anomalous Hall effect. The study holds promise for further increase of T_C using MBE techniques which should enhance Mn incorporation. Ferromagnetic SnTe with high T_C may be of interest in future TCI-based (opto-)electronic devices.[60] Mn doping also favorably modifies the electronic structure via the L and Σ valence band convergence, and synergistically lowers κ by means of enhanced point defect scattering. This leads to an improved TE performance in comparison to undoped SnTe.

[1]J. O. Dimmock, I. Melngailis, and A. J. Strauss, Phys. Rev. Lett. **16**, 1193 (1966).
[2]P. Bauer Pereira, I. Sergueev, S. Gorsse, J. Dadda, E. Müller, and R. P. Hermann, Phys. Status Solidi B **250**, 1300 (2013).
[3]Q. Zhang, B. Liao, Y. Lan, K. Lukas, W. Liu, K. Esfarjani, C. Opeil, D. Broido, G. Chen, and Z. Ren, Proc. Natl. Acad. Sci. U.S.A. **110**, 13261 (2013).

[4]M. Zhou, Z. M. Gibbs, H. Wang, Y. Han, C. Xin, L. Li, and G. J. Snyder, Phys. Chem. Chem. Phys. **16**, 20741 (2014).

[5]G. Tan, L.-D. Zhao, F. Shi, J. W. Doak, S.-H. Lo, H. Sun, C. Wolverton, V. P. Dravid, C. Uher, and M. G. Kanatzidis, J. Am. Chem. Soc. **136**, 7006 (2014).

[6]G. Tan, F. Shi, J. W. Doak, H. Sun, L.-D. Zhao, P. Wang, C. Uher, C. Wolverton, V. P. Dravid, and M. G. Kanatzidis, Energy Environ. Sci. **8**, 267 (2015).

[7]G. Tan, F. Shi, S. Hao, H. Chi, L.-D. Zhao, C. Uher, C. Wolverton, V. P. Dravid, and M. G. Kanatzidis, J. Am. Chem. Soc. **137**, 5100 (2015).

[8]G. Tan, F. Shi, S. Hao, H. Chi, T. P. Bailey, L.-D. Zhao, C. Uher, C. Wolverton, V. P. Dravid, and M. G. Kanatzidis, J. Am. Chem. Soc. **137**, 11507 (2015).

[9]H. Wu, C. Chang, D. Feng, Y. Xiao, X. Zhang, Y. Pei, L. Zheng, D. Wu, S. Gong, Y. Chen *et al.*, Energy Environ. Sci. **8**, 3298 (2015).

[10]J. He, X. Tan, J. Xu, G.-Q. Liu, H. Shao, Y. Fu, X. Wang, Z. Liu, J. Xu, H. Jiang *et al.*, J. Mater. Chem. A **3**, 19974 (2015).

[11]W. Li, Z. Chen, S. Lin, Y. Chang, B. Ge, Y. Chen, and Y. Pei, J. Materiomics **1**, 307 (2015).

[12]G. Tan, W. G. Zeier, F. Shi, P. Wang, G. J. Snyder, V. P. Dravid, and M. G. Kanatzidis, Chem. Mater. **27**, 7801 (2015).

[13]L.-D. Zhao, X. Zhang, H. Wu, G. Tan, Y. Pei, Y. Xiao, C. Chang, D. Wu, H. Chi, L. Zheng *et al.*, J. Am. Chem. Soc. **138**, 2366 (2016).

[14]L.-D. Zhao, S.-H. Lo, Y. Zhang, H. Sun, G. Tan, C. Uher, C. Wolverton, V. P. Dravid, and M. G. Kanatzidis, Nature **508**, 373 (2014).

[15]L.-D. Zhao, G. Tan, S. Hao, J. He, Y. Pei, H. Chi, H. Wang, S. Gong, H. Xu, V. P. Dravid *et al.*, Science **351**, 141 (2016).

[16]K. Peng, X. Lu, H. Zhan, S. Hui, X. Tang, G. Wang, J. Dai, C. Uher, G. Wang, and X. Zhou, Energy Environ. Sci. **9**, 454 (2016).

[17]R. F. Brebrick and A. J. Strauss, Phys. Rev. **131**, 104 (1963).

[18]L. M. Rogers, J. Phys. D: Appl. Phys. **1**, 845 (1968).

[19]J. A. Kafalas, R. F. Brebrick, and A. J. Strauss, Appl. Phys. Lett. **4**, 93 (1964).

[20]T. H. Hsieh, H. Lin, J. Liu, W. Duan, A. Bansil, and L. Fu, Nat. Commun. **3**, 982 (2012).

[21]Y. Tanaka, Z. Ren, T. Sato, K. Nakayama, S. Souma, T. Takahashi, K. Segawa, and Y. Ando, Nat. Phys. **8**, 800 (2012).

[22]L. Fu, Phys. Rev. Lett. **106**, 106802 (2011).

[23]M. Z. Hasan and C. L. Kane, Rev. Mod. Phys. **82**, 3045 (2010).

[24]X.-L. Qi and S.-C. Zhang, Rev. Mod. Phys. **83**, 1057 (2011).

[25]Y. L. Chen, J.-H. Chu, J. G. Analytis, Z. K. Liu, K. Igarashi, H.-H. Kuo, X. L. Qi, S. K. Mo, R. G. Moore, D. H. Lu *et al.*, Science **329**, 659 (2010).

[26]J. G. Checkelsky, J. Ye, Y. Onose, Y. Iwasa, and Y. Tokura, Nat. Phys. **8**, 729 (2012).

[27]I. Lee, C. K. Kim, J. Lee, S. J. L. Billinge, R. Zhong, J. A. Schneeloch, T. Liu, T. Valla, J. M. Tranquada, G. Gu *et al.*, Proc. Natl. Acad. Sci. U.S.A. **112**, 1316 (2015).

[28]C.-Z. Chang, J. Zhang, X. Feng, J. Shen, Z. Zhang, M. Guo, K. Li, Y. Ou, P. Wei, L.-L. Wang *et al.*, Science **340**, 167 (2013).

[29]J. G. Checkelsky, R. Yoshimi, A. Tsukazaki, K. S. Takahashi, Y. Kozuka, J. Falson, M. Kawasaki, and Y. Tokura, Nat. Phys. **10**, 731 (2014).

[30]C. Fang, M. J. Gilbert, and B. A. Bernevig, Phys. Rev. Lett. **112**, 046801 (2014).

[31]A. Haury, A. Wasiela, A. Arnoult, J. Cibert, S. Tatarenko, T. Dietl, and Y. Merle d'Aubigné, Phys. Rev. Lett. **79**, 511 (1997).

[32]P. Sharma, A. Gupta, K. V. Rao, F. J. Owens, R. Sharma, R. Ahuja, J. M. O. Guillen, B. Johansson, and G. A. Gehring, Nat. Mater. **2**, 673 (2003).

[33]H. Ohno, A. Shen, F. Matsukura, A. Oiwa, A. Endo, S. Katsumoto, and Y. Iye, Appl. Phys. Lett. **69**, 363 (1996).

[34]M. E. Overberg, C. R. Abernathy, S. J. Pearton, N. A. Theodoropoulou, K. T. McCarthy, and A. F. Hebard, Appl. Phys. Lett. **79**, 1312 (2001).

[35]T. Story, R. R. Gała̧zka, R. B. Frankel, and P. A. Wolff, Phys. Rev. Lett. **56**, 777 (1986).

[36]Y. D. Park, A. T. Hanbicki, S. C. Erwin, C. S. Hellberg, J. M. Sullivan, J. E. Mattson, T. F. Ambrose, A. Wilson, G. Spanos, and B. T. Jonker, Science **295**, 651 (2002).

[37]Y. S. Hor, P. Roushan, H. Beidenkopf, J. Seo, D. Qu, J. G. Checkelsky, L. A. Wray, D. Hsieh, Y. Xia, S. Y. Xu *et al.*, Phys. Rev. B **81**, 195203 (2010).

[38]M. Inoue, K. Ishii, and H. Yagi, J. Phys. Soc. Jpn. **43**, 903 (1977).

[39]C. W. H. M. Vennix, E. Frikkee, P. J. T. Eggenkamp, H. J. M. Swagten, K. Kopinga, and W. J. M. de Jonge, Phys. Rev. B **48**, 3770 (1993).

[40]H. Chi, W. Liu, K. Sun, X. Su, G. Wang, P. Lošťák, V. Kucek, Č. Drašar, and C. Uher, Phys. Rev. B **88**, 045202 (2013).

[41]A. Arrott, Phys. Rev. **108**, 1394 (1957).

[42]Z. Zhou, Y.-J. Chien, and C. Uher, Appl. Phys. Lett. **87**, 112503 (2005).

[43]G. Wang, L. Endicott, H. Chi, P. Lošťák, and C. Uher, Phys. Rev. Lett. **111**, 046803 (2013).

[44]G. J. Snyder and E. S. Toberer, Nat. Mater. **7**, 105 (2008).

[45]J. P. Heremans, V. Jovovic, E. S. Toberer, A. Saramat, K. Kurosaki, A. Charoenphakdee, S. Yamanaka, and G. J. Snyder, Science **321**, 554 (2008).

[46]H. J. Goldsmid, *Electronic Refrigeration* (Pion, London, 1986).

[47]H. Sun, X. Lu, H. Chi, D. T. Morelli, and C. Uher, Phys. Chem. Chem. Phys. **16**, 15570 (2014).

[48]T. C. Chasapis, Y. Lee, E. Hatzikraniotis, K. M. Paraskevopoulos, H. Chi, C. Uher, and M. G. Kanatzidis, Phys. Rev. B **91**, 085207 (2015).

[49]Y. I. Ravich, B. A. Efimova, and I. A. Smirnov, *Semiconducting Lead Chalcogenides* (Plenum Press, New York, 1970).

[50]D. I. Bilc, S. D. Mahanti, and M. G. Kanatzidis, Phys. Rev. B **74**, 125202 (2006).

[51]H. Wang, E. Schechtel, Y. Z. Pei, and G. J. Snyder, Adv. Energy Mater. **3**, 488 (2013).

[52]S.-H. Wei and A. Zunger, Phys. Rev. B **35**, 2340 (1987).

[53]Y. Z. Pei, X. Y. Shi, A. LaLonde, H. Wang, L. D. Chen, and G. J. Snyder, Nature **473**, 66 (2011).

[54]W. Liu, X. Tan, K. Yin, H. Liu, X. Tang, J. Shi, Q. Zhang, and C. Uher, Phys. Rev. Lett. **108**, 166601 (2012).

[55]H. Sitter, K. Lischka, and H. Heinrich, Phys. Rev. B **16**, 680 (1977).

[56]T. Seddon, S. C. Gupta, and G. A. Saunders, Solid State Commun. **20**, 69 (1976).

[57]E. R. Cowley, J. K. Darby, and G. S. Pawley, J. Phys. C: Solid State Phys. **2**, 1916 (1969).

[58]C. J. Glassbrenner and G. A. Slack, Phys. Rev. **134**, A1058 (1964).

[59]H. Zhang and A. J. Minnich, Sci. Rep. **5**, 8995 (2015).

[60]J. Shen and J. J. Cha, Nanoscale **6**, 14133 (2014).